Acta Crystallographica Section D
Biological Crystallography
ISSN 0907-4449

Structures of feline immunodeficiency virus dUTP pyrophosphatase and its nucleotide complexes in three crystal forms

G. Sridhar Prasad,[a]* Enrico A. Stura,[b] John H. Elder[a] and C. David Stout[a]

[a]Department of Molecular Biology, The Scripps Research Institute, La Jolla, CA 92037-1093, USA, and [b]Departement d'Ingenierie et d'Etudes des Proteines, Bâtiment 152, CEA/Saclay, 91191 Gif-sur-Yvette CEDEX, France

Correspondence e-mail: prasad@scripps.edu

Received 17 March 2000
Accepted 26 June 2000

PDB References: $P6_3$ native dUTPase, 1f7d; $P6_3$ dUMP complex, 1f7k; $P6_3$ dUMP complex (from dUTP), 1f7n; $P2_12_12_1$ native dUTPase, 1f7o; $P2_12_12_1$ dUDP complex, 1f7p; $P2_12_12_1$ dUTP complex, 1f7q; $P2_13$ dUDP complex, 1f7r.

dUTP pyrophosphatase (dUTPase) cleaves the α-β phosphodiester of dUTP to form pyrophosphate and dUMP, preventing incorporation of uracil into DNA and providing the substrate for thymine synthesis. Seven crystal structures of feline immunodeficiency virus (FIV) dUTPase in three crystal forms have been determined, including complexes with substrate (dUTP), product (dUMP) or inhibitor (dUDP) bound. The native enzyme has been refined at 1.40 Å resolution in a hexagonal crystal form and at 2.3 Å resolution in an orthorhombic crystal form. In the dUDP complex in a cubic crystal form refined at 2.5 Å resolution, the C-terminal conserved P-loop motif is fully ordered. The analysis defines the roles of five sequence motifs in interaction with uracil, deoxyribose and the α-, β- and γ-phosphates. The enzyme utilizes adaptive recognition to bind the α- and β-phosphates. In particular, the α-β phosphodiester adopts an unfavorable eclipsed conformation in the presence of the P-loop. This conformation may be relevant to the mechanism of α-β phosphodiester bond cleavage.

1. Introduction

The enzyme dUTP pyrophosphatase (E.C. 3.6.1.23) catalyzes the hydrolysis of dUTP to dUMP and inorganic pyrophosphate. The reaction serves two essential functions in DNA metabolism: the product, dUMP, is the primary source of substrate for synthesis of dTTP, and hydrolysis of dUTP lowers its intracellular concentration, limiting incorporation into DNA (Tye *et al.*, 1977). Misincorporation of uracil leads to strand breaks by uracil DNA glycosylases, observed as Okazaki fragments, in a process termed thymineless cell death (Gadsden *et al.*, 1993). Thus, dUTPase is required not only for the biosynthesis of dTTP, but also for maintaining the integrity of genomic DNA.

FIV is a lentivirus associated with an AIDS-like disease in domestic cats (Ackley *et al.*, 1990). FIV, like other non-primate lentiviruses, including equine infectious anemia virus (EIAV) and visna/maedi viruses of sheep, encodes dUTPase within its *Pol* gene (DU; McClure *et al.*, 1988; McGeoch, 1990; Elder *et al.*, 1992). Herpes viruses (Pedersen *et al.*, 1987) and certain pox viruses (Slabaugh & Roseman, 1989) also contain a DU gene; human endogenous retrovirus encodes a sequence highly homologous to DU (McGeoch, 1990) which may be active during HIV infection.

Because actively dividing cells have relatively high levels of endogenous dUTPase activity, uracil incorporation into viral DNA does not occur to a significant level during replication, even if the virus does not encode dUTPase (Lerner *et al.*,

1995). However, in FIV, EIAV and visna/maedi lentiviruses, the presence of dUTPase is necessary for productive infection of primary macrophages (Lerner *et al.*, 1995; Steagall *et al.*, 1995), which have low endogenous dUTPase activity. Infection in cats with DU^- FIV results in a fivefold increase in the number of mutations in the viral genome (Lerner *et al.*, 1995). Similarly, the mutation rate increases during infection by DU^- caprine arthritis encephalitis virus (Turelli *et al.*, 1996). Consequently, the DU gene stabilizes viral replication in certain cell populations, directly influencing viral host-cell range.

Primary sequences of dUTPases from viral, prokaryotic and eukaryotic species reveal five well conserved motifs (McGeoch, 1990). The conserved C-terminal sequence, motif V, is rich in glycine residues and is termed the P-loop motif. Glycine-rich P-loops of nucleotide-binding enzymes play a critical role in substrate binding and catalysis (Bossemeyer, 1994). However, in dUTPase the role of the P-loop motif has not been clearly established. In available crystal structures of *Escherichia coli*, human, FIV and EIAV dUTPase (Dauter *et al.*, 1998, 1999; Mol *et al.*, 1996; Prasad *et al.*, 1996), motif V is either poorly defined or completely disordered. In this paper, we report seven crystal structures of FIV dUTPase in three lattices, including five complexes with dUMP, dUDP and dUTP. In one dUDP complex motif V is fully ordered. Comparison of these structures and analysis of the α-, β-, and γ-phosphate interactions reveals that at least one function of motif V is to drive the α-β phosphodiester into an unfavorable conformation. This may be relevant to the mechanism of α-β phosphodiester bond cleavage catalyzed by the enzyme.

2. Materials and methods

2.1. Protein preparation and crystallization

FIV dUTPase was expressed and purified as previously described (Prasad *et al.*, 1996). Crystallization experiments followed the principles of reverse screening (Stura *et al.*, 1994) in combination with streak- and macro-seeding techniques (Stura & Wilson, 1991). Crystals of the hexagonal ($P6_3$) form were grown by sitting-drop vapor diffusion in a constant-temperature incubator at 295 K from a 21 mg ml^{-1} protein solution in 5 m*M* $MgCl_2$, 2 m*M* β-mercaptoethanol, 50 m*M* Tris–HCl pH 7.5. Drops consisted of 3.5 µl of protein solution and 2.5 µl of a reservoir solution consisting of 13% MPEG 5K, 50 m*M* sodium cacodylate pH 6.5. Crystals appeared in about 50% of drops; crystals were obtained from the remaining drops by macro-seeding. The crystals are hexagonal prisms 0.3 × 0.3 mm in width, with a variable length of 0.3–0.7 mm. Crystals of the orthorhombic ($P2_12_12_1$) form were grown in a similar manner, using a reservoir solution of 1.0 *M* sodium citrate pH 6.5. The crystals are rectangular prisms 0.2 × 0.4 × 0.6 mm in size. Crystals of the cubic ($P2_13$) form were grown by pre-incubating a 16 mg ml^{-1} protein solution in 25 m*M* dUDP, 5 m*M* $MgCl_2$ and 2 m*M* β-mercaptoethanol, 50 m*M* Tris–HCl pH 7.0 for 16 h. The protein solution was then used for crystallization as for the hexagonal and orthorhombic forms, with 1.25 *M* sodium citrate pH 6.5 as the reservoir solution. The crystals are cubic prisms 0.3 mm on an edge.

2.2. Data collection

A low-temperature native data set for the $P6_3$ crystal form was collected by briefly transferring the crystal to synthetic mother liquor containing 25% ethylene glycol and then flash-freezing the crystal at 100 K. A complete data set to 1.40 Å resolution was collected at Stanford Synchrotron Radiation Laboratory beamline 7-1 (λ = 1.08 Å) using a 34.5 cm MAR Research image-plate scanner. Six data sets were collected at 291 K using a Siemens SRA X-ray generator operated at 50 kV, 100 mA and equipped with a graphite monochromator and a 30 cm MAR Research image-plate scanner. Crystals were mounted in thin-walled glass capillaries in synthetic mother liquor. All data sets were indexed, integrated, merged and scaled using *MOSFLM* and the *CCP*4 program suite (Collaborative Computational Project, Number 4, 1994) (Table 1).

2.3. High-resolution refinement in the $P6_3$ crystal form

The high-resolution native structure in the hexagonal crystal form (Table 2) was refined using the 1.9 Å structure as a starting model (Prasad *et al.*, 1996). The model was subjected to rigid-body, positional, simulated-annealing and *B*-factor refinement against the low-temperature data using *CNS* (Adams *et al.*, 1997). Non-crystallographic restraints were not applied. $2|F_o| - |F_c|$ and $|F_o| - |F_c|$ electron-density maps were used to correct and adjust the model with *TURBO FRODO* (Jones *et al.*, 1991). The model was then refined using *SHELX*97 (Sheldrick & Schneider, 1997). Distance, planarity, chiral volume and anti-bumping restraints were applied and the list of reflections used for $R_{\rm free}$ calculations was unchanged. Solvent molecules and two Mg^{2+} ions, one on the threefold axis of each independent trimer, were added after three rounds of refinement. Anisotropic *B* factors were introduced during the fifth round and were restrained to have similar values for spatially adjacent atoms. $2|F_o| - |F_c|$ and $|F_o| - |F_c|$ electron-density maps were used to correct and adjust the model following all subsequent rounds. Nine rounds of *SHELX* refinement were performed, with the final round including the working as well as the $R_{\rm free}$ data set.

2.4. Structure determination and refinement in the $P2_12_12_1$ and $P2_13$ crystal forms

The orthorhombic and cubic structures (native and dUDP complex, respectively; Table 2) were solved by molecular replacement using *AMoRe* (Navaza, 1994) with the structure in the hexagonal crystal form as a search model. Cross rotation-function and translation-search calculations yielded clear solutions in each case. For the orthorhombic structure, rigid-body refinement resulted in a correlation coefficient of 0.61 and an *R* factor of 0.41 for one dUTPase trimer in the asymmetric unit. For the cubic structure, rigid-body refinement resulted in a correlation coefficient of 0.66 and an *R* factor of 0.36 for one dUTPase trimer on the crystallographic

Table 1
Crystallographic parameters and data-collection statistics.

Crystal form	Hexagonal			Orthorhombic			Cubic
Complex	Native (100 K)	dUMP	dUMP (from dUTP)	Native	dUDP	dUTP	dUDP
Space group	$P6_3$	$P6_3$	$P6_3$	$P2_12_12_1$	$P2_12_12_1$	$P2_12_12_1$	$P2_13$
Unit-cell parameters (Å)							
a	77.07	79.12	79.35	68.29	68.77	68.35	72.44
b	77.07	79.12	79.35	71.70	72.00	71.65	72.44
c	86.17	87.12	87.31	77.04	77.28	76.92	72.44
Asymmetric unit (subunits)	2	2	2	3	3	3	1
Solvent content (%)	49	56	41	41	41	41	41
V_m (Å^3 Da^{-1})	2.46	2.77	2.77	2.10	2.10	2.10	2.10
All data							
Resolution (Å)	1.40	2.20	2.20	2.20	2.28	2.26	2.50
Total observations	212437	72884	88228	62046	65258	51135	10960
Unique reflections	55495	15105	15858	18956	19893	18741	4414
Completeness (%)	97.1	92.9	95.0	96.1	99.3	95.5	96.4
$R_{\rm symm}$ (%)	3.8	4.0	5.2	7.1	7.8	5.8	10.4
$I/\sigma(I)$	11.1	15.6	12.6	4.4	6.8	2.0	11.1
Last shell							
Resolution (Å)	1.44–1.40	2.28–2.20	2.28–2.20	2.26–2.20	2.36–2.28	2.32–2.26	2.59–2.50
Completeness (%)	82.3	42.7	58.1	94.0	100.0	93.7	92.5
$R_{\rm symm}$ (%)	20.4	28.8	34.8	40.5	63.5	45.9	24.6
$I/\sigma(I)$	3.1	2.7	1.6	1.1	1.1	1.5	4.5

threefold axis. Both structures were refined using *CNS* as for the native structure in the hexagonal crystal form. Solvent molecules were fitted to $\geq 3.0\sigma$ peaks in $|F_o| - |F_c|$ maps within 2.4–3.8 Å of hydrogen-bonding donor or acceptor protein atoms. During refinement $>2\sigma$ density was apparent in unbiased $|F_o| - |F_c|$ maps for the C-terminal 16 residues of the independent subunit in the cubic crystal form (Fig. 1*a*); these residues are disordered in both independent subunits in the hexagonal crystal form and in all three independent subunits in the orthorhombic crystal form (Table 2). These residues were modeled based on the primary sequence (Talbott *et al.*, 1989) and refined. Unbiased density was also apparent for dUDP (Fig. 2*c*), consistent with the crystallization conditions, and for Mg^{2+} on the threefold axis. These moieties were also included in the model and refined (Table 2).

2.5. Refinement of nucleotide complexes

Soaking experiments using the $P6_3$ and $P2_12_12_1$ crystal forms resulted in four active-site complexes (Table 2). One of the dUMP complexes resulted from turnover of dUTP during soaking, presumably because $MgCl_2$, which is required for catalysis, was present in the buffer. Hexagonal crystals soaked in dUDP invariably cracked and could not be used for data collection. dUDP and dUTP complexes of the orthorhombic crystal form were obtained (Table 2). dUDP is a dUTPase inhibitor (Larsson *et al.*, 1996) and dUTP was presumably not hydrolyzed because sodium citrate in the crystallization medium can chelate Mg^{2+}.

The native structures in the hexagonal and orthorhombic crystal forms were used as starting models for refinement against the respective data sets for soaked crystals, following the same procedures as applied to the native structures. Examination of unbiased $|F_o| - |F_c|$ electron-density maps clearly revealed the presence of the bound nucleotides (Figs. 2*a*, 2*b* and 2*d*). While both independent active sites were occupied in the dUMP complexes in the hexagonal crystal form, only two of three independent active sites were occupied in the dUDP and dUTP complexes in the orthorhombic crystal form. The nucleotides, solvent molecules and metal ions were included and the structures were refined as for the native structures (Table 2).

2.6. Crystal packing

The $P6_3$ crystal form contains independent trimers on the 6_3 screw and threefold axes. The interface between non-crystallographically related subunits contains several charged residues and a number of water molecules. Three water molecules are directly hydrogen bonded to atoms of both subunits; another 15 are involved in interactions where two or more bridge between the subunits. There are four direct contacts involving residues Asp10, Lys11 and Arg95 of one subunit and Thr91, Arg95, Glu96 and Lys97 of the other.

The $P2_12_12_1$ crystal form contains a complete dUTPase trimer in the asymmetric unit. Interactions between the carbonyl group of Arg87 and symmetry-related amides of Gln113 occur for each of the three independent subunits. There are no other significant contacts in this crystal form. In the $P2_13$ crystal form the trimer packs on the crystallographic threefold axis. In this case, Phe133 in the ordered C-terminus participates in hydrophobic contacts with symmetry-related subunits. In addition, two hydrogen-bond interactions stabilize the cubic lattice, one involving Arg87 and Gln113, as in the orthorhombic lattice, and the other the amide N atom of Leu111 and the side chain of Asp10.

3. Results and discussion

3.1. FIV dUTPase crystal structures

dUTPase is a functional trimer in which three active sites are formed by the arrangement of five conserved sequence motifs from all three subunits; *e.g.* motifs I, II and IV from subunit *A*, motif III from subunit *B* and motif V from subunit *C* form one active site at the interface of subunits *A* and *B* (Fig. 1*b*). Crystal structures of *E. coli* (Cedergren-Zeppezauer *et al.*, 1992; Larsson *et al.*, 1996; Dauter *et al.*, 1998), human (Mol *et al.*, 1996), FIV (Prasad *et al.*, 1996) and EIAV (Dauter *et al.*, 1999) dUTPases have been determined. Complexes with dUMP, dUDP and dUTP have been studied in the human enzyme and with dUDP in the *E. coli* and EIAV enzymes. In

Table 2
Refinement statistics.

	Hexagonal			Orthorhombic			Cubic
	Native (100 K)	dUMP	dUMP (from dUTP)	Native	dUDP	dUTP	dUDP
Soaking conditions							
Nucleotide	None	dUMP	dUTP	None	dUDP	dUTP	dUDP
Concentration (m*M*)	—	20	10	—	10	10	25
Time (h)	—	72	24	—	17	24	Co-crystallized
Model							
Subunit *A* (residues)	118	116	116	116	116	116	133
Subunit *B* (residues)	117	116	116	116	116	116	—
Subunit *C* (residues)	—	—	—	116	116	116	—
Nucleotide (moles)	—	dUMP (2)	dUMP (2)	—	dUDP (2)	dUTP (2)	dUDP (1)
Refinement							
Resolution (Å)	20.0–1.40	50.0–2.20	50.0–2.20	10.0–2.30	15.0–2.30	30.0–2.30	50.0–2.50
Reflections	48461	14409	14461	17229	18154	16935	3778
R factor ($\|F_o\| \geq 2\sigma_F$)	0.178	0.221	0.216	0.216	0.221	0.232	0.192
$R_{\rm free}$ (% of reflections)	0.228 (3.0)	—	—	0.286 (5.8)	—	—	0.266 (10.0)
Geometry							
Bonds (Å)	0.008	0.010	0.011	0.011	0.009	0.013	0.013
Angles (°)	1.77	1.48	1.60	1.55	1.48	1.76	1.72
Dihedrals (°)	29.6	29.8	29.5	30.9	30.5	30.9	30.3
Average *B* factors (Å^2)							
Protein (atoms)	27.1 (1792)	30.8 (1776)	32.7 (1776)	25.6 (2635)	27.5 (2635)	25.2 (2635)	24.8 (1006)
Nucleotide (atoms)	—	27.5 (40)	36.0 (40)	—	37.2 (48)	35.6 (56)	25.5 (24)
Mg^{2+} (atoms)	9.8 (2)	23.9 (2)	32.7 (2)	—	—	—	36.0 (1)
Solvent (atoms)	37.2 (185)	35.9 (133)	36.7 (80)	33.8 (201)	35.7 (96)	30.6 (129)	47.3 (54)

this paper, seven structures of FIV dUTPase are reported in three crystal forms that include six independent copies of the protein subunit, 16 copies of the enzyme active site and nine dUMP, dUDP or dUTP complexes (Table 2). In the hexagonal crystal form the trimers lie on threefold and 6_3 screw axes, defining two crystallographic independent subunits and active sites. In the orthorhombic crystal form a complete trimer occupies the asymmetric unit. In the cubic crystal form the trimer lies on a threefold axis, defining one crystallographic independent subunit and active site. This crystal form provides the first example of a fully ordered structure for motif V. These structures allow the interactions of the uracil, deoxyribose and phosphate groups to be analyzed in different crystal-packing environments and compared with nucleotide complexes in dUTPases from other species. The comparisons confirm highly specific recognition of uracil and deoxyribose and reveal adaptive recognition of the α- and β-phosphates.

3.2. High-resolution native structure

The 1.40 Å resolution structure in the hexagonal crystal form (Table 2) is the highest resolution refinement of a dUTPase to date. No significant differences are observed in the conformation and hydrogen-bonding interactions of active-site and conserved-motif residues compared with the previously reported structure refined at 1.9 Å (Prasad *et al.*, 1996). Interactions between the independent copies of the protein subunits are better defined and a number of additional ordered H_2O molecules are observed. However, the C-terminal residues of motif V (residues 118–133) remain disordered at 100 K. These residues are not visible in the crystal structures of the *E. coli* and EIAV enzymes and their dUDP complexes (Dauter *et al.*, 1998, 1999) and are highly mobile in the human enzyme, with *B* factors in the range 70–100 Å^2 (Mol *et al.*, 1996), suggesting that the motif V P-loop is conformationally dynamic.

3.3. Native structure in orthorhombic crystals

The asymmetric unit of the orthorhombic crystal form contains a functional trimer (Table 2). The structure of the subunit and the interactions within the trimer are very similar to the structure in the hexagonal crystal form. As in the hexagonal crystal form, the C-terminal 17 residues are disordered. Pairwise least-squares superposition of 114 residues in the five independent protein subunits in the hexagonal and orthorhombic crystal forms results in r.m.s. deviations in the range 0.44–1.23 Å for C^α atoms and 0.94–1.52 Å for all atoms. The only distinct difference is the absence of a Mg^{2+} ion on the threefold axis, in contrast to the hexagonal crystal form where Asp64 from three subunits and three H_2O molecules coordinate to Mg^{2+} (Prasad *et al.*, 1996). The absence of Mg^{2+} is presumably a consequence of crystallization in 1.0 *M* sodium citrate, which can chelate Mg^{2+} in the buffer. Instead, an H_2O molecule occupies the site and forms hydrogen bonds ($\sim$2.7 Å) with the OD1 atoms of Asp64 from the three subunits. The absence of Mg^{2+} may be related to the lower crystal symmetry, although the crystallization conditions are very different.

3.4. dUDP complex in cubic crystals

Cubic crystals of FIV dUTPase were grown in the presence of the inhibitor dUDP with sodium citrate as the precipitant. Under these conditions an ordered conformation of the C-terminal 17 residues is captured in the crystal lattice (Fig. 1*a*;

Table 2). These residues adopt an extended conformation and make a number of specific contacts with the other two subunits before reaching the interface of the adjacent and remote subunits, completing formation of the active site (Fig. 1*b*). Details of these contacts are shown in Figs. 1(*c*) and 1(*d*); they include 13 hydrogen bonds, eight involving main chain groups, and four salt bridges, one involving the C-terminal carboxyl group. The conformational switch from an 'open' (disordered) to a 'closed' state, as observed in the cubic crystal lattice,

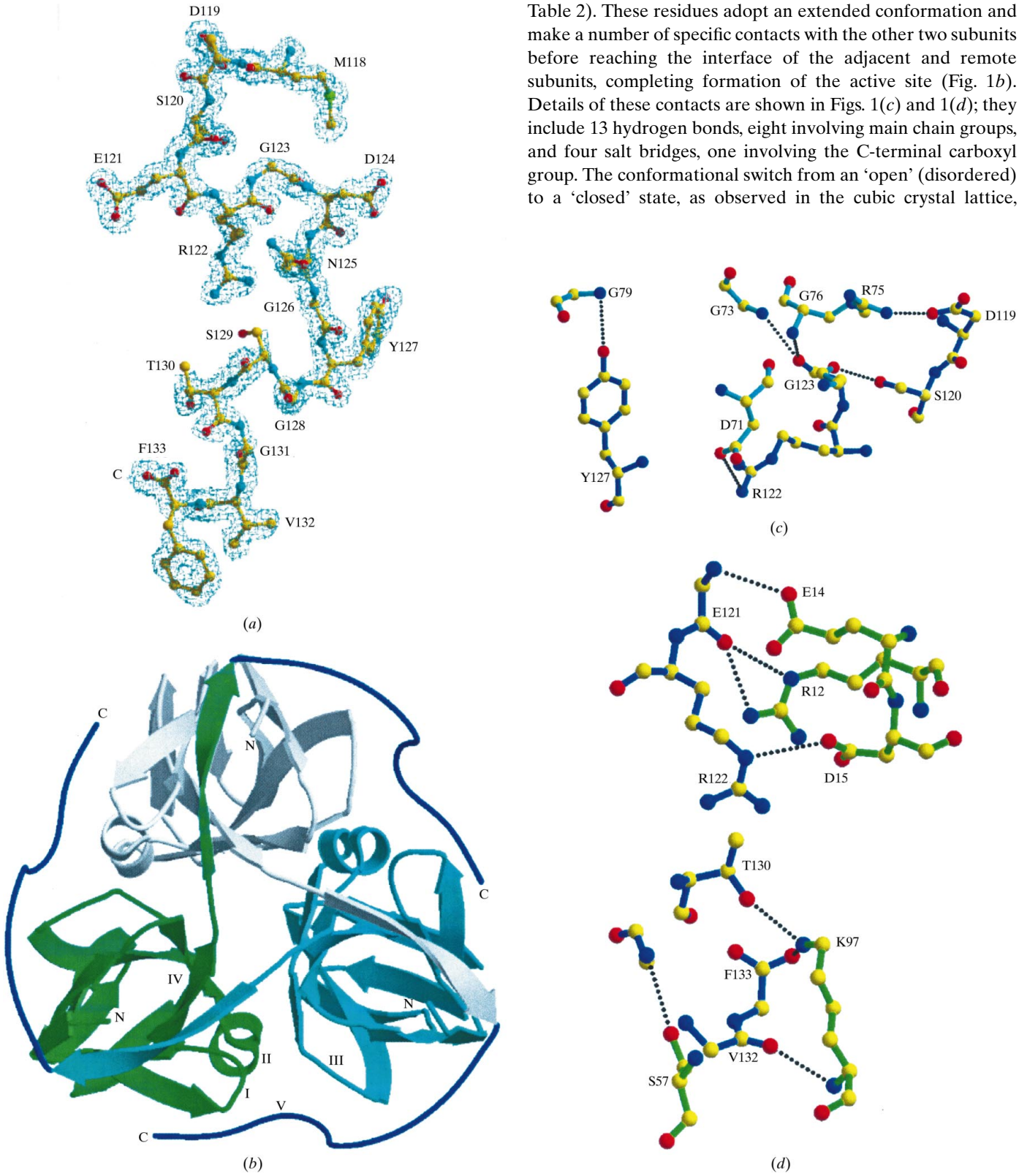

Figure 1
(*a*) Electron density for the ordered C-terminal 16 residues (motif V) of FIV dUTPase with dUDP bound in the cubic crystal form. The map was computed with $2|F_o| - |F_c|$ coefficients following simulated-annealing refinement and phase calculation in which residues 118–133 were omitted. All atoms of residues Met118–Phe133 are shown. The map is contoured at 1.0σ. (*b*) The FIV dUTPase trimer viewed down the threefold axis, showing the ordered C-terminal residues (motif V) in relation to the other two subunits. Conserved sequence motifs are indicated for one of the active sites, which is composed of motifs I, II and IV from one subunit (green), motif III from a second subunit (cyan) and motif V (blue) from the third subunit (gray). (*c*) Details of the interactions of the ordered C-terminus (blue bonds) with residues in the domain containing motif III (cyan bonds). (*d*) Details of the interactions of the ordered C-terminus (blue bonds) with residues in the domain containing motifs I, II and IV (green bonds).

appears to be a critical feature of the catalytic cycle (Vertessy *et al.*, 1998).

No Mg^{2+} ion is observed in the proximity of the active site, perhaps because of the lower resolution of this structure and the absence of the γ-phosphate. Nonetheless, an Mg^{2+} site is observed as a 5σ peak on the threefold axis of the trimer, coincident with the threefold axis of the $P2_13$ space group, in spite of the presence of sodium citrate in the crystallization medium. The Mg^{2+} is octahedrally coordinated to Asp64 and three H_2O molecules as in the hexagonal crystal structure. Hence, three trimers on crystallographic 6_3-screw and threefold axes bind Mg^{2+}, whereas a trimer in an asymmetric unit (orthorhombic form) does not (Table 2). The protein subunit in the cubic crystal form is very similar to those in the hexagonal and orthorhombic crystal forms, with r.m.s. deviations ranging from 0.51 to 0.92 Å for C^{α} atoms and 0.96 to 1.24 Å for all atoms.

In the crystal structure of the dUDP complex of EIAV dUTPase an Sr^{2+} ion is observed in the active site, but motif V remains disordered (Dauter *et al.*, 1999). In the cubic crystal form motif V is ordered but there is no metal ion. These results are consistent with solution studies of the *E. coli* enzyme, which show that formation of the active site, *i.e.* ordering of the P-loop, requires the triphosphate moiety and Mg^{2+} (Vertessy *et al.*, 1998). A metal ion coordinated to α- and γ-phosphates has been modeled in the dUTP complex of human dUTPase (Mol *et al.*, 1996).

3.5. dUMP, dUDP and dUTP complexes in hexagonal and orthorhombic crystals

The dUMP complexes in the hexagonal crystal form are virtually identical (Table 2). One is the result of turnover of dUTP during soaking in the presence of Mg^{2+}. The binding of

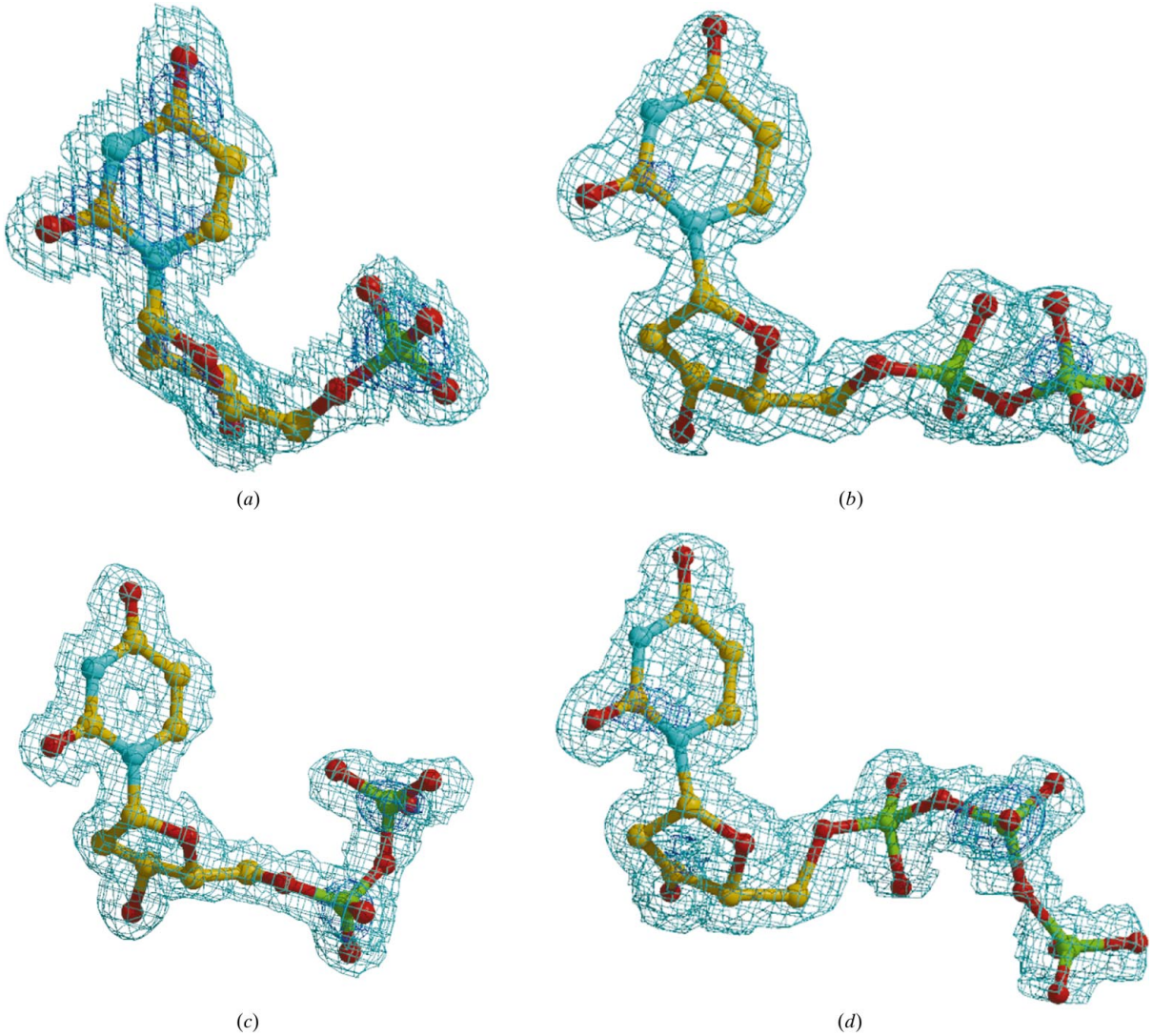

Figure 2
Electron density for nucleotides in four unique FIV dUTPase complexes in three crystal forms (Table 2). The maps were computed with $2|F_o| - |F_c|$ coefficients following simulated-annealing refinement and phase calculation in which the nucleotides were omitted. The maps are contoured at 1.0 and 3.0σ. (*a*) The dUMP complex in the hexagonal crystal form. Copy *A* of the complex prepared by soaking in dUMP is shown. (*b*) The dUDP complex in the orthorhombic crystal form (copy *A* is shown). (*c*) The dUDP complex in the cubic crystal form. (*d*) The dUTP complex in the orthorhombic crystal form (copy *A* is shown).

dUMP does not induce conformational change in motif V. The dUDP and dUTP complexes in the orthorhombic crystal form were also obtained by soaking (Table 2). The orthorhombic crystal form displays asymmetry in that the active sites of the trimer are unequally occupied (Table 2). However, the C-terminal residues remain disordered for all subunits. dUTP binding without hydrolysis is consistent with the absence of Mg^{2+} in the orthorhombic crystal form. Disorder in motif V is also consistent with the requirement that both Mg^{2+} and the γ-phosphate be present to assemble the active site.

3.6. Recognition of uracil and deoxyribose

Specific recognition of uracil and deoxyribose is accomplished by residues in motif III which form a β-hairpin between strands $\beta5$ and $\beta6$ (Fig. 3*a*). Main-chain amide and carbonyl groups form hydrogen bonds with O2, N3 and O4 of uracil and a trapped H_2O molecule. The conserved residue Asp71 hydrogen bonds with O3′ of the sugar; the conserved residue Tyr74, which hydrogen bonds across the β-hairpin, stacks on C2′ of deoxyribose. These interactions are essentially identical for all nine copies of dUMP, dUDP and dUTP (Table 2) and are the same as observed in complexes of the human, *E. coli* and EIAV enzymes (Mol *et al.*, 1996; Larsson *et al.*, 1996; Dauter *et al.*, 1999). Consequently, specific recognition of the base and sugar is conserved in viral, prokaryotic and eukaryotic dUTPases. When motif V is ordered, Tyr127, a conserved aromatic residue in FIV dUTPase, stacks over the uracil ring (Fig. 3*b*). This interaction is similar to the 'Phe-lid' seen in dUMP, dUDP and dUTP complexes of human dUTPase (Mol *et al.*, 1996) and apparently serves to retain the substrate prior to hydrolysis.

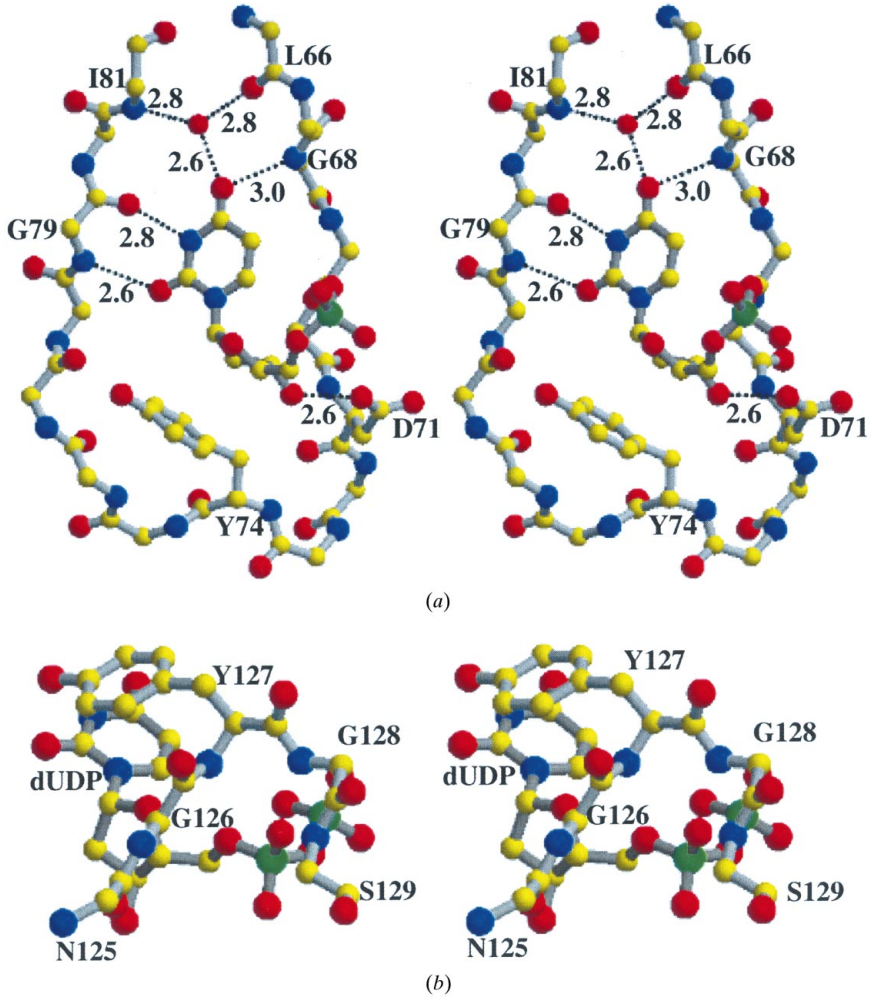

Figure 3
(*a*) Stereoview of the β-hairpin between strands $\beta5$ and $\beta6$ of the FIV dUTPase protein subunit that comprises motif III. Specific recognition of uracil occurs *via* hydrogen bonding with main-chain amide and carbonyl groups and a trapped H_2O molecule (red). Specific recognition of deoxyribose occurs *via* stacking of Tyr74 and hydrogen bonding with Asp71. Recognition of the base and sugar is the same in all dUMP, dUDP and dUTP complexes. (*b*) Stereoview of the C-terminal residues 125–129 in the dUDP complex in the cubic crystal form. Residues 127–129 make several hydrogen bonds with the α-phosphate (Fig. 4*c*), while the side chain of Tyr127 stacks on the uracil ring.

3.7. Phosphate interactions

Interaction with the phosphate groups occurs *via* motifs II and IV in the subunit adjacent to motif III and *via* motif V from the third subunit. Motif II contains the conserved sequence Lys55-Ser56-Ser57, motif IV contains the conserved basic residue Lys97 and motif V contains the conserved residues Arg122 and Tyr127-Gly128-Ser129 (Prasad *et al.*, 1996). Interactions of these residues with the phosphates in four unique types of complexes are depicted in Fig. 4: dUMP in the hexagonal crystal form (Fig. 4*a*), dUDP in the orthorhombic crystal form (Fig. 4*b*), dUDP in the cubic crystal form (Fig. 4*c*) and dUTP in the orthorhombic crystal form (Fig. 4*d*). Redundant copies of these unique complexes (Table 2) are essentially the same as shown in Fig. 4.

The motifs accommodate alternate conformations of the α- and β-phosphates. In the dUMP complex the α-phosphate interacts with Lys55, Ser56 and two H_2O molecules (Fig. 4*a*). In the dUDP complex these interactions are retained and Ser56 and Ser57 hydrogen bond with the β-phosphate (Fig. 4*b*). In the dUDP complex in the presence of motif V there is a significant rearrangement: Lys55, Ser56 and Ser57 now interact exclusively with the β-phosphate and the α-phosphate acquires six new hydrogen bonds from motif V, involving the amides of Tyr127, Gly128 and Ser129 and the side chains of Arg122 and Ser129 (Fig. 4*c*). In the dUTP complex, interactions of the α- and β-phosphates resemble

those in the dUDP complex in the absence of motif V and Lys55 and Lys97 hydrogen bond with the γ-phosphate (Fig. 4*d*).

The function of the motifs can be generalized: in the absence of motif V, motif II recognizes both the α- and β-phosphates; in the presence of motif V, motif II recognizes the β-phosphate and motif V recognizes the α-phosphate; motifs II and IV recognize the γ-phosphate. Similar roles for the conserved motifs are observed in the dUDP complexes of *E. coli* and EIAV dUTPase (Larsson *et al.*, 1996; Dauter *et al.*, 1999) and in the dUTP complex of human dUTPase (Mol *et al.*, 1996). In EIAV dUTPase with Sr^{2+} bound, motif II interacts exclusively with the β-phosphate, as in FIV when motif V is ordered. In human dUTPase the interactions of motif V with the α-phosphate are similar to those in FIV dUTPase. The EIAV and human complexes manifest features required for catalysis (metal ion, γ-phosphate bound) and therefore may resemble catalytically relevant conformations. Because motif–phosphate interactions are similar in EIAV, human and FIV dUTPases, the dUDP complex with motif V ordered should also represent a catalytically relevant conformation.

3.8. Induced strain in the α-β phosphodiester

Comparisons imply that binding of motif V positions the α-β phosphodiester for catalysis. Because substrate must bind prior to ordering of the C-terminal residues over the active site, initial interaction of the α- and β-phosphates may be as in Fig. 4(*b*). Subsequent binding of motif V to the α-phosphate would then displace motif II, promoting new interactions with the β-phosphate and altering the conformation about the α-β phosphodiester (Fig. 4*c*).

Fig. 5(*a*) shows the superposition of the nucleotides in the unique FIV dUTPase complexes. The positioning of α-phosphate groups is similar in all four complexes, as is that of the β-phosphate in the dUDP and dUTP complexes in the

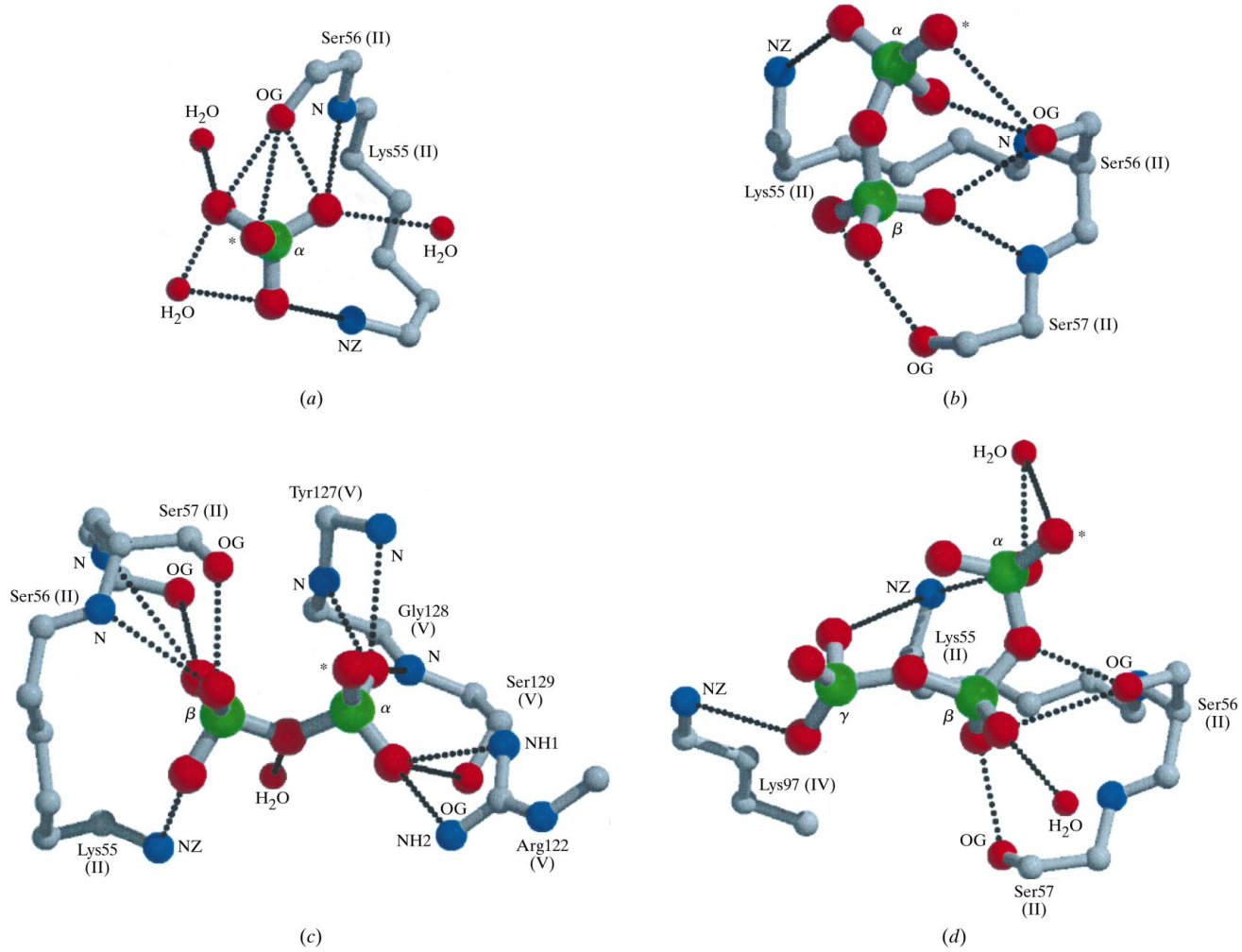

Figure 4
Interaction between FIV dUTPase and the phosphate groups of nucleotides in four unique complexes in three crystal forms (Table 2). Potential hydrogen bonds (dotted lines) are indicated for all contacts $\leq$3.5 Å between phosphate O atoms and protein atoms and for ordered H_2O molecules. The asterisk indicates the O5′ atom linking the α-phosphate to deoxyribose of the nucleotides. Roman numerals indicate the conserved sequence motifs to which the residues belong. (*a*) The dUMP complex in the hexagonal crystal form. Copy *A* of the complex prepared by soaking in dUMP is shown. (*b*) The dUDP complex in the orthorhombic crystal form (copy *A* is shown). (*c*) The dUDP complex in the cubic crystal form. (*d*) The dUTP complex in the orthorhombic crystal form (copy *A* is shown). For clarity, interactions of the α-phosphate with motif V are not shown.

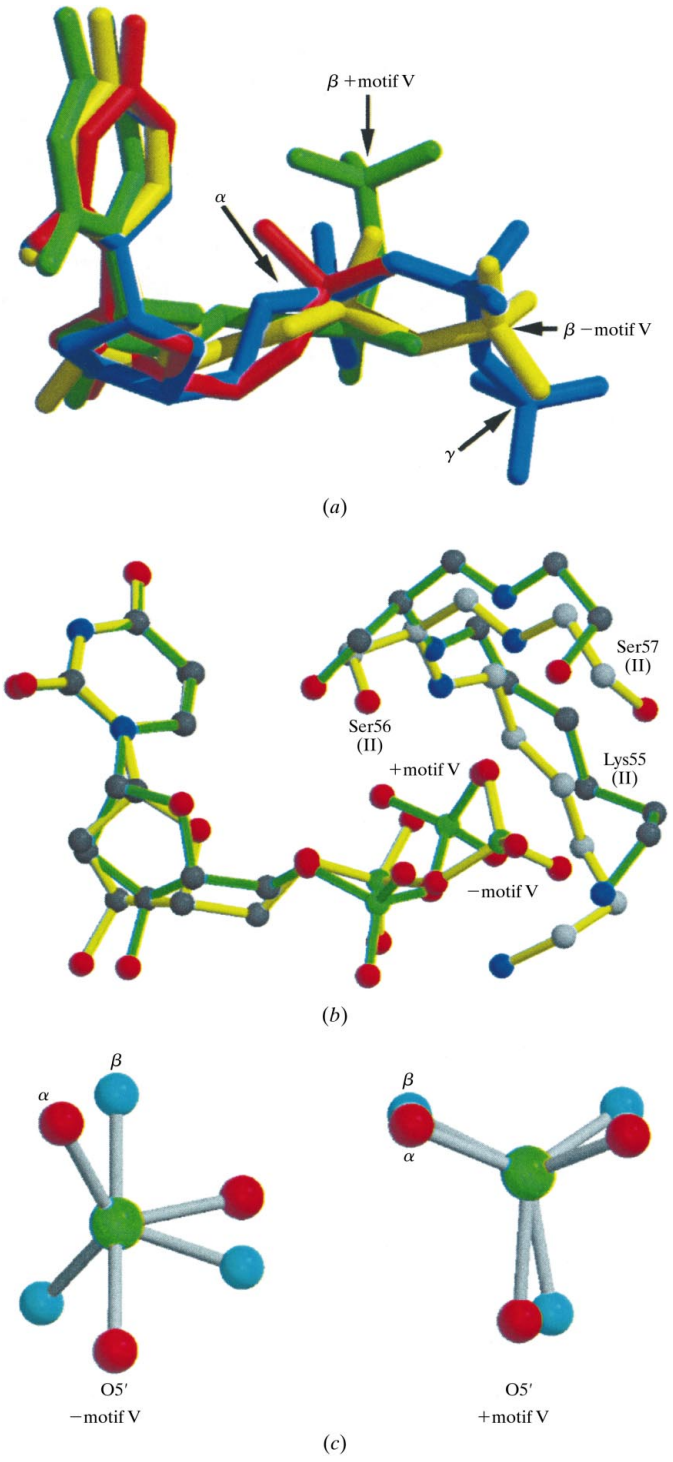

Figure 5
(*a*) Superposition of the nucleotides in four unique complexes in three crystal forms of FIV dUTPase (Table 2): dUMP (red), dUDP in the absence of motif V (yellow), dUDP in the presence of motif V (green), dUTP (blue). Binding of motif V induces a large change in the conformation about the α-β phosphodiester, repositioning the β-phosphate. (*b*) Superposition of the dUDP complexes in the orthorhombic crystal form (yellow bonds) and the cubic crystal form (green bonds), showing the repositioning of motif II residues to accommodate the two conformations of the β-phosphate. (*c*) Staggered and eclipsed conformations of the α-β phosphodiester in the absence (left) and presence (right) of motif V. O atoms of the α-phosphate group, including the O5′ atom of deoxyribose, are shown in red; O atoms of the β-phosphate are shown in cyan; for clarity, the linking phosphodiester O atom is not shown.

orthorhombic crystal form. However, ordering of motif V in the dUDP complex in the cubic crystal form causes the phosphate backbone to adopt a folded rather than an extended conformation, resulting in a large shift in the position of the β-phosphate. In this case, the α-β phosphodiester is in a left-handed screw conformation (Sheffer & Trueblood, 1965). The concomitant rearrangement of motif II residues associated with this alternate conformation of the β-phosphate is shown by superposition in Fig. 5(*b*).

The O atoms of the α-β phosphodiester are staggered in the absence of motif V (Fig. 5*c*). Similarly, a staggered conformation is observed in the EIAV and human dUTPase complexes, in which the C-terminal residues are disordered or have very high *B* factors (Dauter *et al.*, 1999; Mol *et al.*, 1996). However, in the presence of motif V the O atoms become eclipsed (Fig. 5*c*). This conformation would be expected to increase electrostatic repulsion between the phosphate O atoms, introducing strain into the phosphodiester and favoring hydrolysis. Therefore, it appears that the eclipsed conformation of the α-β phosphodiester could represent a transition state and that a function of motif V is to induce this strained conformation by promoting interaction of motif II with the β-phosphate.

The authors wish to thank Peter Kuhn, Mike Soltis and Aina Cohen for their generous help at Stanford Synchrotron Radiation Laboratory beamline 7-1. This work was supported by NIH grants GM48495 (to CDS) and AI25825 and MH47680 (to JHE).

References

Ackley, C. D., Yamamoto, J. K., Levy, N., Pedersen, N. C. & Cooper, M. D. (1990). *J. Virol.* **64**, 5652–5655.
Adams, P. D., Pannu, N. S., Read, R. J. & Brünger, A. T. (1997). *Proc. Natl Acad. Sci. USA*, **94**, 5018–5023.
Bossemeyer, D. (1994). *Trends Biochem. Sci.* **19**, 201–205.
Cedergren-Zeppezauer, E. S., Larsson, G., Nyman, P. O., Dauter, Z. & Wilson, K. S. (1992). *Nature (London)*, **355**, 740–743.
Collaborative Computational Project, Number 4 (1994). *Acta Cryst.* D**50**, 760–763.
Dauter, Z., Persson, R., Rosengren, A. M., Nyman, P. O., Wilson, K. S. & Cedergren-Zeppezauer, E. S. (1999). *J. Mol. Biol.* **285**, 655–673.
Dauter, Z., Wilson, K. S., Larsson, G., Nyman, P. O. & Cedergren-Zeppezauer, E. S. (1998). *Acta Cryst.* D**54**, 735–749.
Elder, J. H., Lerner, D. L., Hasselkus-Light, C. S., Fontenot, D. J., Hunter, E., Luciw, P. A., Montelaro, R. C. & Phillips, T. R. (1992). *J. Virol.* **66**, 1791–1794.
Gadsden, M. H., McIntosh, E. M., Game, J. C., Wilson, P. J. & Haynes, R. H. (1993). *EMBO J.* **12**, 4425–4431.
Jones, T. A., Zou, J. Y., Cowan, S. W. & Kjeldgaard, M. (1991). *Acta Cryst.* A**47**, 110–119.
Larsson, G., Svensson, L. A. & Nyman, P. O. (1996). *Nature Struct. Biol.* **3**, 532–538.
Lerner, D. L., Wagaman, P. C., Phillips, T. R., Prospero-Garcia, O., Henrisksen, S. J., Fox, H. S., Bloom, F. E. & Elder, J. H. (1995). *Proc. Natl Acad. Sci. USA*, **92**, 7480–7484.
McClure, M. A., Johnson, M. S., Feng, D.-F. & Doolittle, R. F. (1988). *Proc. Natl Acad. Sci. USA*, **85**, 2469–2473.

McGeoch, D. J. (1990). *Nucleic Acids Res.* **18**, 4105–4110.
Mol, C. D., Harris, J. M., McIntosh, E. M. & Tainer, J. A. (1996). *Structure*, **4**, 1077–1092.
Navaza, J. (1994). *Acta Cryst.* A**50**, 157–163.
Pedersen, N. C., Ho, E. W., Brown, M. L. & Yamamoto, J. K. (1987). *Science*, **235**, 790–793.
Prasad, G. S., Stura, E. A., McRee, D. E., Laco, G. S., Hasselkus-Light, C., Elder, J. H. & Stout, C. D. (1996). *Protein Sci.* **5**, 2429–2437.
Sheffer, E. & Trueblood, K. N. (1965). *Acta Cryst.* **18**, 1067–1077.
Sheldrick, G. M. & Schneider, T. R. (1997). *Methods Enzymol.* **276**, 319–343.
Slabaugh, M. B. & Roseman, N. A. (1989). *Proc. Natl Acad. Sci. USA*, **86**, 4152–4155.
Steagall, W. K., Robek, M. D., Perry, S. T., Fuller, F. J. & Payne, S. L. (1995). *Virology*, **210**, 302–313.
Stura, E. A., Satterthwait, A. C., Calvo, J. C., Kaslow, D. C. & Wilson, I. A. (1994). *Acta Cryst.* D**50**, 448–455.
Stura, E. A. & Wilson, I. A. (1991). *J. Cryst. Growth*, **110**, 270–282.
Talbott, R. L., Sparger, E. E., Lovelace, K. M., Fitch, W. M., Pedersen, N. C., Luciw, P. A. & Elder, J. H. (1989). *Proc. Natl Acad. Sci. USA*, **86**, 5743–5747.
Turelli, P., Petursson, G., Guigan, F., Mornex, J.-F., Vigne, R. & Querat, G. (1996). *J. Virol.* **70**, 1213–1217.
Tye, B.-K., Nyman, P. O., Lehman, I. R., Hochhauser, S. & Weiss, B. (1977). *Proc. Natl Acad. Sci. USA*, **74**, 154–157.
Vertessy, B. G., Larsson, G., Persson, T., Bergman, A. C., Persson, R. & Nyman, P. O. (1998). *FEBS Lett.* **421**, 83–88.